

Article

Flatness-Based Active Disturbance Rejection Control for a PVTOL Aircraft System with an Inverted Pendular Load

Cesar Alejandro Villaseñor Rios ^{1,†} , Alberto Luviano-Juárez ^{1,†} , Norma Beatriz Lozada-Castillo ^{1,†} , Blanca Esther Carvajal-Gómez ^{1,†} , Dante Mújica-Vargas ^{2,†}  and Octavio Gutiérrez-Frías ^{1,*} 

¹ Instituto Politécnico Nacional, Unidad Profesional Interdisciplinaria en Ingeniería y Tecnologías Avanzadas, Mexico City 07340, Mexico; cvillasenorr0900@alumno.ipn.mx (C.A.V.R.); aluvianoj@ipn.mx (A.L.-J.); nlozadac@ipn.mx (N.B.L.-C.); becarvajal@ipn.mx (B.E.C.-G.)

² TecNM-CENIDET, Cuernavaca, Morelos, 62490, Mexico; dante.mv@cenidet.tecnm.mx

* Correspondence: ogutierrezf@ipn.mx

† These authors contributed equally to this work.

Abstract: This paper presents a systematic procedure for the control scheme design for a PVTOL aircraft system with an inverted pendular load, which is a nonlinear underactuated system. The control scheme is based on the use of angular movement as an artificial control in order to propose new auxiliary control inputs. This is achieved by a linear extended state observer-based active disturbance rejection control to reject both nonmodeled dynamics and external disturbances. The flying planar inverted pendulum is then linearized around an unstable equilibrium point, and the resulting system is subdivided into two subsystems: (1) the height system, and (2) the horizontal pendulum system. For the height system, a linear extended state observer-based active disturbance rejection control is proposed in order to accomplish a take-off and landing task in the presence of external disturbances and non-linearities neglected in the linearization process. The flatness property in the horizontal-pendulum system is exploited in order to propose another active disturbance rejection control of linear nature. The flatness of the tangentially linearized model provides a unique structural property that results in an advantageous low-order cascade decomposition of the linear extended state observer design. Numerical simulations show the effectiveness of the proposed control scheme in trajectory tracking tasks in the presence of disturbances caused by crosswinds with random amplitudes.

Keywords: underactuated systems; inverted pendulum; unmanned aerial vehicle; active disturbance rejection control; nonlinear control; robust control



Citation: Villaseñor Rios, C.A.; Luviano-Juárez, A.; Lozada-Castillo, N.B.; Carvajal-Gómez, B.E.; Mújica-Vargas, D.; Gutiérrez-Frías, O. Flatness-Based Active Disturbance Rejection Control for a PVTOL Aircraft System with an inverted Pendular Load. *Machines* **2022**, *10*, 595. <https://doi.org/10.3390/machines10070595>

Academic Editor: Tao Li

Received: 22 June 2022

Accepted: 19 July 2022

Published: 21 July 2022

Publisher's Note: MDPI stays neutral with regard to jurisdictional claims in published maps and institutional affiliations.



Copyright: © 2022 by the authors. Licensee MDPI, Basel, Switzerland. This article is an open access article distributed under the terms and conditions of the Creative Commons Attribution (CC BY) license (<https://creativecommons.org/licenses/by/4.0/>).

1. Introduction

The analysis and control of underactuated systems (UAS) is an active and intricate research topic in automatic control theory [1] because control inputs cannot produce arbitrary accelerations in some of the degrees of freedom at every instant in time [2]. This fact has several untoward consequences for design control laws. For instance, some UAS are not linearizable by static or dynamic feedback, making most of the traditional control schemes inapplicable. In contrast, the need for fewer actuators in UAS produces some practical advantages like lighter structures, lower costs, and reduced dimensions [3]; these have permitted the practical use of UAS in real applications such as damping systems [4], aerial vehicles [5], ground vehicles [6], and flexible robots [7], among others.

A classical benchmark in automatic control theory is the inverted pendulum system (IPS), which includes the pendubot, acrobot, wheeled inverted pendulum, spherical inverted pendulum, Furuta pendulum and, in recent years, the flying inverted pendulum. All these systems are nonlinear, underactuated, and unstable mechanical systems and many control strategies have been developed for stabilization and tracking the use of linear and non-linear control. Furuta et al. [8] are concerned with attitude control of a triple inverted

pendulum system in which the lower hinge is free for rotation and two upper hinges are controlled. The controller is designed by using a linearized model in a neighbourhood of the upright position; simulations and experimental results are shown. In [9], robustness improvement in a class of UAS is addressed by combining the so-called IDA-PBC controller with an adaptive control technique. This control scheme is used in the inertia wheel inverted pendulum with numerical simulations and real-time experiments. The proposal in [10] leads global stabilization for the cart-pendulum system by control strategy based on the use of saturation functions. Aguilar-Ibañez et al. [11] present a non-linear controller for the stabilization of the Furuta pendulum by using a partial feedback linearisation. In the first stage, only the actuated coordinate is linearised; then, the stabilizing feedback controller is achieved by applying the Lyapunov direct method. This paper proves local asymptotic stability and demonstrates that the closed-loop system has a large region of attraction.

In recent decades, some popular UAS include the unmanned aerial vehicle (UAV) because of its robust electro-mechanical design, high maneuverability, and low cost; moreover, their use can be applied to various fields, such as environmental monitoring, terrain mapping, emergency response, and military use, among others [12]. This wide diversity of applications has motivated novel device configurations, instrumentation schemes, and research in control theory to apply linear and nonlinear controls. Classical linear control is based on an approximate linear model near the equilibrium point, and many examples of linear control can be found in the literature, including the proportional integral derivative (PID) control [13] and linear quadratic regulator (LQR) control [14,15] for stabilization and tracking problems. In addition, some interesting works can be found related to nonlinear control approaches for UAS stabilization and tracking. In Hernández et al. [16], a control strategy is developed for take-off and landing maneuvers in a Quadcopter system. The control strategy consists of a combination of controllers based on nested saturations and a generalized proportional integral (GPI) controller, and it is designed considering the presence of disturbances. Consequently, larger robustness is obtained and the algorithm convergence is proven by means of Lyapunov's second method. Azinheira et al. [17] present a backstepping-based controller used on the UAV system with input saturation, and the stability of the control solution is verified. Another backstepping approach is showcased by Das et al. [18], in which the backstepping approach is used for the quadrotor controller on the Lagrangian form of the dynamics; in addition, two neural networks are introduced to estimate the aerodynamic components. The proposed controller shows robustness cope of unmodeled disturbances. Xiong et al. [19] apply a second-order sliding mode control approach to design a robust flight controller for the Quadcopter system, which is designed to provide a robust position and attitude tracking control with respect to model parameter uncertainties.

Planar vertical take-off and landing (PVTOL) has been used as a benchmark for many research works given that it represents a simplification of other UAV systems, such as Quadcopter and aircraft. PVTOL is a hardly nonlinear control problem because it is an underactuated, nonminimum phase system and, due to the moment-to-force coupling in the model, its zero dynamic is unstable, and the exact input-output linearization methodology produces undesirable results. Numerous works about stabilization control for the PVTOL system can be located in the literature. Hauser et al. [20] showed a model extension in the PVTOL system and proposed a state feedback linearization control for stabilization. In [21], the state feedback control technique in a PVTOL extended model is analyzed, and the conditions under which it is possible to determine local asymptotic stability by using a control based on feedback linearization is found. In [22], Fantoni et al. proposed a global stabilizing scheme for the PVTOL system considering PVTOL's angle as a fictitious control input. The control scheme is formed by a nonlinear combinations of linear saturation functions bounding the thrust input and the rolling moment. Global convergence of the state is proved. An extension of this work is shown in [23] wherein robustness is proven with respect to lateral force coupling, which was neglected in the previous work.

The robust control design for UAV systems is an active and challenging problem for stabilization and tracking given that these kinds of systems are subjected to disturbance in outdoor applications due to wind; consequently, there is a vast amount of literature on the subject. In [24], a backstepping procedure is applied to control the height position together with the nested saturation functions controller for horizontal position and roll angle stabilization, and an extended state observer is used to estimate the wind disturbance. In [25], a robust control strategy to stabilize a PVTOL aircraft in the presence of crosswind is proposed by the use of robust control Lyapunov functions (RCLF) and Sontag's universal stabilizing feedback.

In recent years, the flying inverted pendulum (FIP) system has attracted interest in automatic control research; this system consists of an inverted pendulum linked to a UAV system. The FIP system was developed by Hehn and D'Andrea [26] in 2011. The LQR control was used to stabilize the position of the pendulum and Quadcopter systems considering that the pendulum's mass was less than 5% of the UAV's mass. Some other works have been developed based on the FIP system by using different control ideas; a three-level cascade strategy is proposed in [27], wherein each level of the cascade system executes a control law designed through a backstepping approach and numerical simulations were carried out. Chen et al. [28] used an improved genetic algorithm to determine parameters in the LQR controller in order to get better stabilization in the FIP system. Numerical simulations were carried out to observe the performance of the control methodology proposed. In [29], a backstepping control law based on geometric principles to swing up the FIP system is proposed, and numerical experiments have shown control actions for aggressive maneuvers.

The active disturbance rejection control (ADRC) has led to a new paradigmatic control vision whereby external and internal disturbances are actively estimated and rejected from a simplified version of the system. The ADRC field exhibits an increasing number of experimental results in diverse applications. In [30], a robust trajectory tracking control for the PVTOL system under crosswind is discussed. The control proposed is a combination of input–output feedback linearization and ADRC to estimate and compensate the crosswind effects. In [31], a three-loop cascade control strategy based on ADRC is proposed for the FIP system. Simulation results showed a comparison to an LQR controller to illustrate the robustness of the control proposal. A flatness-based approach is proposed for the linear ADRC stabilization of a nonlinear inertia wheel pendulum in [32], which is subject to unmodelled dynamics and external disturbances. The approach exploits the cascade structure of the tangential linearization of the underactuated system and design a high-gain linear cascaded extended state observer of the generalized proportional integral type. Experimental results are shown to demonstrate the effectiveness and feasibility of the proposed approach with respect to a classic control technique.

The aforementioned works use restriction in the pendulum's mass considered in [26]. Consequently, the pendulum's dynamics are neglected in the UAV's dynamics and, in fact, the flying pendulum system is in the presence of external disturbances produced by wind, as reported in above. Considering works in the literature, this paper is focused on the trajectory-tracking problem and stabilization in the PVTOL aircraft system with an inverted pendular load under crosswind disturbances without restriction in the pendulum's mass. This consideration causes coupling in the pendulum and UAV dynamics. This work explores the differential flatness property in the PVTOL aircraft system with an inverted pendular load in order to design a control scheme that consists of three closed-loop controls; in each one, a linear state feedback control law is proposed, derived from differential flatness system, and an extended state observer (ESO) to estimate and compensate the crosswind is applied. In addition, this proposal considers that only position is available in state measurement. Consequently, the control scheme proposed takes advantage of the ESO to estimate the states that are not directly available for measurements.

The main contributions of this study are as follows:

- (i) a control strategy that uses the differential flatness property in the PVTOL aircraft system with an inverted pendular load in order to design a control for the height, roll attitude, horizontal position, and roll angle simultaneously, even in the presence of a crosswind;
- (ii) a control algorithm, which is robust against the presence of external disturbances and whose performance is competitive with respect to another robust controller of discontinuous nature; and
- (iii) a set of convenient transformations (cascade structure [3]), in which the linearized high-order system can be expressed as a various tandem lower-order systems depending on measurable variables that allow a controller formed by the combination of linear extended state observer-based ADRCs.

The rest of this article is divided as follows. In Section 2 the PVTOL aircraft system with an inverted pendular load is described, and the mathematical model is derived by using Euler–Lagrange formalism. Section 3 is devoted to describing the proposed control approach in four subsections. Section 3.1 presents the control loop for roll angle and a normalized form of the system. Section 3.2 shows the height control, and Section 3.3 presents the control loop for horizontal displacement and pendulum’s angle. Section 4 is devoted to numerical simulations, and Section 5 presents the conclusions.

2. Mathematical Model

The PVTOL aircraft system with an inverted pendulum attached to the PVTOL’s center of gravity is a mechanical system that consists in a PVTOL vehicle and an inverted pendulum attached to the PVTOL’s center of gravity; this system is a two-dimensional version of the FIP system. PVTOL aircraft system with an inverted pendular load is shown in Figure 1, and its dynamical model is derived by Euler–Lagrange equations. The Lagrangian of the system is constructed by the difference of the kinetic and potential energies of the PVTOL and the inverted pendulum,

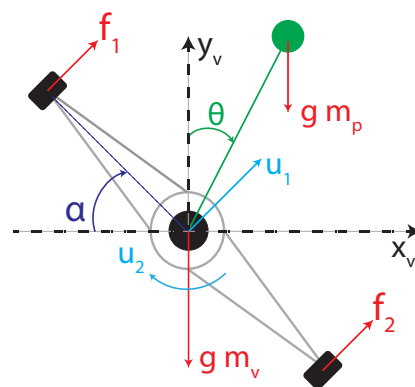


Figure 1. PVTOL aircraft system with an inverted pendular load.

$$\mathcal{K}_v = \frac{m_v \dot{\epsilon}_v \dot{\epsilon}_v^T}{2} + \frac{i_v \dot{\alpha}^2}{2} \quad \mathcal{K}_p = \frac{m_p \dot{\epsilon}_p \dot{\epsilon}_p^T}{2} + \frac{i_p \dot{\theta}^2}{2}$$

$$\mathcal{P}_v = m_v g y_v \quad \mathcal{P}_p = m_p g (l_p \cos(\theta) + y_v)$$

where m_v is the PVTOL’s mass, m_p is the pendulum’s mass, i_v is the PVTOL’s inertia, i_p is the pendulum’s inertia and l_p is the pendulum’s length, $\epsilon_v = (x_v, y_v)$ is the reference frame fixed to PVTOL’s center of gravity related to an inertial reference frame fixed in the ground. ϵ_p is the reference frame fixed to pendulum’s center of gravity and it is related to ϵ_v as

$$\epsilon_p = \epsilon_v^T + R_\theta [0 \quad l_p]^T$$

R_θ is the rotational matrix defined as

$$R_\theta = \begin{bmatrix} \cos(\theta) & -\sin(\theta) \\ \sin(\theta) & \cos(\theta) \end{bmatrix}$$

The Lagrangian of the PVTOL aircraft system with an inverted pendular load is defined as follows:

$$\mathcal{L} = \frac{-2gl_p m_p \cos(\theta) - 2g(m_v + m_p)y_v + (m_v + m_p)(\dot{x}_v^2 + \dot{y}_v^2)}{2} + \frac{i_v \dot{\alpha}^2 - 2l_p m_p (\cos(\theta)\dot{x}_v + \sin(\theta)\dot{y}_v)\dot{\theta} + (i_p + l_p^2 m_p)\dot{\theta}^2}{2}. \quad (1)$$

By using Euler–Lagrange formalism, the dynamics can be calculated as

$$\frac{d}{dt} \frac{\partial \mathcal{L}}{\partial \dot{q}} - \frac{\partial \mathcal{L}}{\partial q} = U + d, \quad (2)$$

where q is the generalized coordinates vector of the system, $q = [x_v \ y_v \ \alpha \ \theta]^\top$, U and d are the control inputs matrix and the external disturbance matrix defined as follows:

$$U = [-u_1 \sin(\alpha) \quad u_1 \cos(\alpha) \quad u_2 \quad 0]^\top$$

$$d = [-d_x \sin(\alpha) \quad d_y \cos(\alpha) \quad d_\alpha \quad 0]^\top.$$

Control inputs u_1 and u_2 are defined through the forces generated by the pairs propeller-motor of PVTOL, $u_1 = f_1 + f_2$ and $u_2 = f_2 - f_1$ and disturbances are taken as crosswind inputs as shown in [30] with amplitudes d_x , d_y , and d_α respectively.

By solving the Euler–Lagrange Equation (2), differential equations of the system can be expressed as $M(q)\ddot{q} + C(q, \dot{q})\dot{q} + G(q) = U + d$, where matrix $M(q)$ is symmetric and non-singular, $C(q, \dot{q})$ is the Coriolis matrix, and $G(q)$ is the gravity vector. Solving this expression for \ddot{q} , the dynamical system can be expressed as

$$\ddot{q} = M^{-1}(q)(U - C(q, \dot{q})\dot{q} - G(q)) + M^{-1}(d). \quad (3)$$

Without loss of generality, PVTOL's structure is taken as a rigid body, the pendulum is assumed as a rigid massless bar with a point mass in its end, $i_p = 0$, and PVTOL's inertia is $i_v = 1$. Solving the expression (3) for the Lagrangian described in (1) of the PVTOL aircraft system with an inverted pendular load, the following differential equations are obtained:

$$\ddot{x}_v = \frac{-0.5u_1((2m_v + m_p)\sin(\alpha) + m_p \sin(\alpha) + 2\theta) + l_p m_v m_p \sin(\theta)\dot{\theta}^2}{m(m_v + m_p)} + D_x \quad (4)$$

$$\ddot{y}_v = \frac{-2gm_v(m_v + m_p) + (2m_v + m_p)u_1 \cos(\alpha) - m_p u_1 \cos(\alpha + 2\theta) + 2l_p m_v m_p \cos(\theta)\dot{\theta}^2}{2m_v(m_v + m_p)} \quad (5)$$

$$+ D_y \quad (6)$$

$$\ddot{\alpha} = u_2 + D_\alpha \quad (7)$$

$$\ddot{\theta} = \frac{u_1 \sin(\alpha + \theta)}{l_p m_v} + D_\theta \quad (8)$$

with

$$D_x = - \frac{0.5d_x(2m_v + m_p + m_p \cos(2\theta)) \sin(\theta) + d_y m_p \cos(\alpha) \cos(\theta) \sin(\theta)}{m_v(m_v + m_p)} \tag{9}$$

$$D_y = \frac{d_y \cos(\alpha)(2m_v + m_p - m_p \cos(2\theta)) + d_x m_p \sin(\alpha) \sin(2\theta)}{2m_v(m_v + m_p)} \tag{10}$$

$$D_\alpha = d_\alpha \tag{11}$$

$$D_\theta = \frac{d_x \cos(\theta) \sin(\alpha) + d_y \cos(\alpha) \sin(\theta)}{l_p m_v} \tag{12}$$

Control problem. Consider the PVTOL aircraft system with an inverted pendular load dynamical system ((4)– (8)). The problem is to design a control scheme for a take-off and landing maneuver while ensuring the stabilization in the inverted pendulum position around the unstable equilibrium point, through the control inputs u_1 and u_2 in spite of the presence of disturbances caused by crosswind and nonmodeled dynamics.

3. Control Scheme

The control scheme is conformed by three control loops: The first loop is designed for the trajectory tracking control in α angle. This inner loop keeps the trajectory tracking error in a sufficiently small vicinity of the origin to consider the desired trajectory as an artificial control in the PVTOL aircraft system with an inverted pendular load, where new auxiliary controllers are proposed. The PVTOL aircraft system with an inverted pendular load is tangentially linearized around the unstable equilibrium point, and the linearized system is used to design the second and third control loops. The second loop is devoted to trajectory tracking for take-off and landing maneuvers, and the third loop explores the differential flatness property in the horizontal displacement and pendulum’s angle system in order to stabilize both coordinates at the same time. A diagram of the proposed control scheme is depicted in Figure 2.

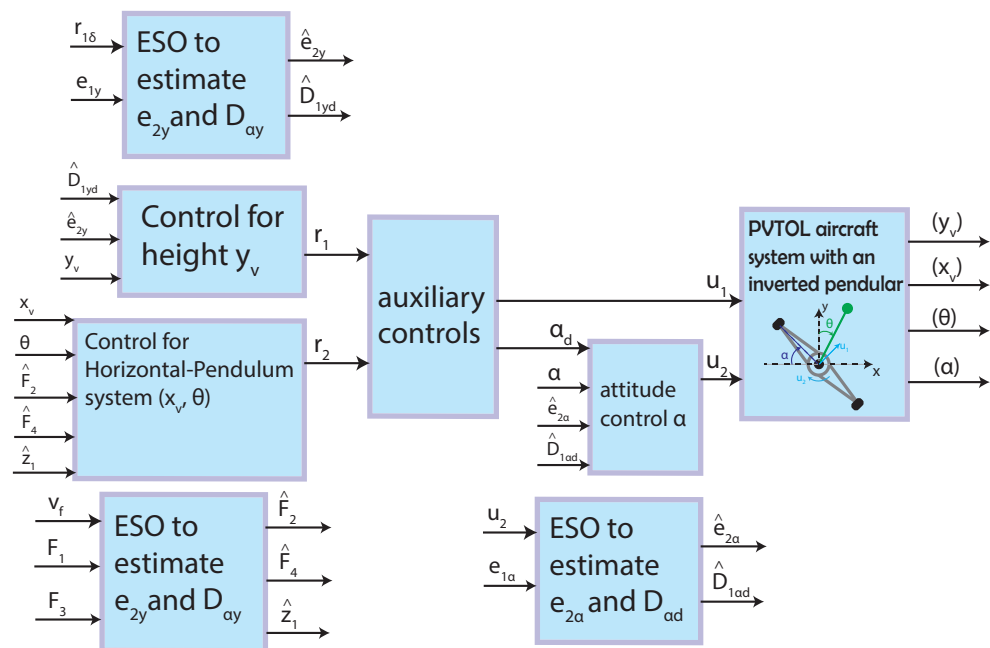


Figure 2. Schematics of the control scheme.

The following assumptions are considered for the control design.

Assumption 1. The time derivatives of the desired trajectory for α angle are not well known.

Assumption 2. Only linear and angular positions are available for measurement.

3.1. Control for α Angle

Dynamics for the α angle are described by Equations (7) and (11). Where disturbance d_α is caused by crosswind and is uniformly absolutely bounded, it is assumed that there exists a finite constant such that $\|d_\alpha\| < \delta_\alpha$. The control objective is to keep α close to the desired trajectory, α_d , which will be calculated by the following control loops; consequently, only the desired trajectory is known, but its time derivatives are not. Defining the trajectory tracking error $e_\alpha = \alpha_d - \alpha$ and expressing the dynamical trajectory tracking error in terms of state variables $e_{1\alpha} = e_\alpha$ and $e_{2\alpha} = \dot{e}_\alpha$, the dynamical equations of the trajectory tracking error are expressed as follows:

$$\dot{e}_{1\alpha} = e_{2\alpha} \quad (13)$$

$$\dot{e}_{2\alpha} = \ddot{\alpha}_d - u_2 - D_\alpha. \quad (14)$$

By Assumption 1 $\ddot{\alpha}_d$ is not well known, so it will be taken as disturbance, $D_{\alpha_d} = \ddot{\alpha}_d - D_\alpha$. It is clear that the nondisturbed system, i.e., $D_{\alpha_d} = 0$, (13), (14) is a pure integrator chain.

In order to reject the disturbance D_{α_d} , and to achieve Assumption 2, the following ESO is proposed for simultaneous estimation of $e_{2\alpha}$ and the disturbance signal D_{α_d} :

$$\dot{\hat{e}}_{1\alpha} = \hat{e}_{2\alpha} + \lambda_{1\alpha}(e_{1\alpha} - \hat{e}_{1\alpha}) \quad (15)$$

$$\dot{\hat{e}}_{2\alpha} = u_2 + \lambda_{2\alpha}(e_{1\alpha} - \hat{e}_{1\alpha}) + \hat{D}_{1\alpha_d}$$

$$\dot{\hat{D}}_{1\alpha_d} = \hat{D}_{2\alpha_d} + \lambda_{3\alpha}(e_{1\alpha} - \hat{e}_{1\alpha})$$

$$\dot{\hat{D}}_{2\alpha_d} = \lambda_{4\alpha}(e_{1\alpha} - \hat{e}_{1\alpha}).$$

The observation error of the state variable $O_\alpha = e_{1\alpha} - \hat{e}_{1\alpha}$ is subject to the following linearly dominant reconstruction error dynamics:

$$O_\alpha^{(4)} + \lambda_{1\alpha}O_\alpha^{(3)} + \lambda_{2\alpha}\ddot{O}_\alpha + \lambda_{3\alpha}\dot{O}_\alpha + \lambda_{4\alpha}O_\alpha = \zeta_\alpha.$$

The term ζ_α represents the total uniformly absolutely bounded disturbance due to external disturbances and internal perturbations, i.e., $\|\zeta_\alpha\| < \delta_1\zeta$. A necessary and sufficient condition for having the observation error O_α ultimately, uniformly, convergent toward a sufficiently small neighborhood of the acceleration estimation error phase space [3,33], consists in choosing the observer control parameters, $\lambda_{j\alpha}$ $j = 1, 2, 3, 4$, such that the characteristic polynomial associated with the linear dominant dynamics is Hurwitz, making the linear injection error dynamics stable. The controller is thus given by

$$u_2 = k_{\alpha 1}e_{1\alpha} + k_{\alpha 2}\hat{e}_{2\alpha} - \hat{D}_{1\alpha_d}, \quad (16)$$

where $e_{1\alpha}$ is measurable and, is used instead of its estimate. The trajectory tracking error dynamics of the closed loop is given by

$$\ddot{e}_\alpha + k_{\alpha 2}\dot{e}_\alpha + k_{\alpha 1}e_\alpha = \eta_\alpha, \quad (17)$$

where $\eta_\alpha = \|D_{\alpha_d} - \hat{D}_{\alpha_d}\| < K_\alpha$. The control parameters $k_{\alpha 1}$ and $k_{\alpha 2}$ are chosen such that a stable second-order dynamics with characteristic polynomial $s^2 + 2\omega_0\zeta_0s + \omega_0^2$, being $\omega_n, \zeta_0 \in \mathbb{R}^2$, is matched. In this case, the control parameters are chosen as $k_{\alpha 1} = \omega_0^2$ and $k_{\alpha 2} = 2\omega_0\zeta_0$. This means that angle α tends to be close to the desired trajectory α_d in a sufficiently small neighborhood after a finite time t_α , so

$$\lim_{t \rightarrow \infty} |e_\alpha| < K_\alpha.$$

Linearized PVTOL Aircraft System with an Inverted Pendular Load

According to [16], after applying control u_2 (16) and a later finite time t_α , the trajectory tracking error, e_α , is sufficiently close to zero; consequently, it is possible to replace α for α_d and use it as artificial control input [10,22,23] for the PVTOL aircraft system with an inverted pendular load, where the error between α and α_d is taken as a disturbance input in the subsequent control loop. Proposing control inputs u_1 and α_d as

$$\begin{aligned} u_1 &= \sqrt{r_1^2 + r_2^2} \\ \alpha_d &= \arctan(r_2/r_1), \end{aligned} \tag{18}$$

the PVTOL aircraft system with an inverted pendular load is expressed as follows:

$$\ddot{x}_v = -\frac{r_2(2m_v + m_p + m_p \cos(2\theta)) + m_p r_1 \sin(2\theta) - 2l_p m_v m_p \sin(\theta) \dot{\theta}^2}{2m_v(m_v + m_p)} + D_x \tag{19}$$

$$\begin{aligned} \ddot{y}_v &= \frac{-2gm_v(m_v + m_p) + (2m_v + m_p)r_1 - m_p r_1 \cos(2\theta)}{2m_v(m_v + m_p)} \\ &+ \frac{m_p r_2 \sin(2\theta) + l_p m_v m_p \cos(\theta) \dot{\theta}^2}{2m_v(m_v + m_p)} + D_y \end{aligned} \tag{20}$$

$$\ddot{\theta} = \frac{r_2 \cos(\theta) + r_1 \sin(\theta)}{l_p m_v} + D_\theta \tag{21}$$

where

$$D_x = \frac{-d_x(m_v + m_p)r_2 + m_p \sin(\theta)(-d_y r_1 \cos(\theta) + d_x r_2 \sin(\theta))}{m_v(m_v + m_p)\sqrt{r_1^2 + r_2^2}} \tag{22}$$

$$D_y = \frac{d_y r_1(m_v + m_p - m_p \cos(\theta)^2) + d_x m_p r_2 \cos(\theta) \sin(\theta)}{m_v(m_v + m_p)\sqrt{r_1^2 + r_2^2}} \tag{23}$$

$$D_\theta = \frac{d_x r_2 \cos(\theta) + d_y r_1 \sin(\theta)}{l_p m_v \sqrt{r_1^2 + r_2^2}}. \tag{24}$$

Equations (19)–(21) represent the reduced dynamical model of the PVTOL aircraft system with an inverted pendular load with r_1 and r_2 as control inputs.

A desired equilibrium point is given by: $x_v = 0, y_v = 0, \dot{x}_v = 0, \dot{y}_v = 0, \theta = 0, \dot{\theta} = 0, r_1 = g(m_v + m_p), r_2 = 0$; consequently, defining state variables $x_1 = x, x_2 = \dot{x}, y_1 = y, y_2 = \dot{y}, \theta_1 = \theta, \theta_2 = \dot{\theta}$ and performing a tangent linearization of the system (19)–(21) [3], the resulting dynamics, ignoring disturbances, can be described in following form:

$$\begin{bmatrix} \dot{x}_{1\delta} \\ \dot{x}_{2\delta} \\ \dot{y}_{1\delta} \\ \dot{y}_{2\delta} \\ \dot{\theta}_{1\delta} \\ \dot{\theta}_{2\delta} \end{bmatrix} = \begin{bmatrix} 0 & 1 & 0 & 0 & 0 & 0 \\ 0 & 0 & 0 & 0 & -\frac{gm_p}{m_v} & 0 \\ 0 & 0 & 0 & 1 & 0 & 0 \\ 0 & 0 & 0 & 0 & 0 & 0 \\ 0 & 0 & 0 & 0 & 0 & 1 \\ 0 & 0 & 0 & 0 & \frac{g(m_v + m_p)}{l_p m_v} & 0 \end{bmatrix} \begin{bmatrix} x_{1\delta} \\ x_{2\delta} \\ y_{1\delta} \\ y_{2\delta} \\ \theta_{1\delta} \\ \theta_{2\delta} \end{bmatrix} + \begin{bmatrix} 0 & 0 \\ 0 & -\frac{1}{m_v} \\ 0 & 0 \\ 1 & 0 \\ \frac{1}{m_v + m_p} & 0 \\ 0 & 0 \\ 0 & \frac{1}{l_p m_v} \end{bmatrix} \begin{bmatrix} r_{1\delta} \\ r_{2\delta} \end{bmatrix}, \tag{25}$$

where $[x_{1\delta} \ x_{2\delta} \ y_{1\delta} \ y_{2\delta} \ \theta_{1\delta} \ \theta_{2\delta}]^T$ are the incremental state variables of the linear system, and $[r_{1\delta} \ r_{2\delta}]^T$ are the incremental control inputs. The linear system (25) can be separated into two parts: the height subsystem ($y_{1\delta}$) and the horizontal pendulum subsystem ($x_{1\delta}, \theta_{1\delta}$) as

$$\begin{bmatrix} \dot{y}_{1\delta} \\ \dot{y}_{3\delta} \end{bmatrix} = \begin{bmatrix} 0 & 1 \\ 0 & 0 \end{bmatrix} \begin{bmatrix} y_{1\delta} \\ y_{3\delta} \end{bmatrix} + \begin{bmatrix} 0 \\ 1 \\ m_v + m_p \end{bmatrix} r_{1\delta} \quad (26)$$

$$\begin{bmatrix} \dot{x}_{1\delta} \\ \dot{x}_{2\delta} \\ \dot{\theta}_{1\delta} \\ \dot{\theta}_{2\delta} \end{bmatrix} = \begin{bmatrix} 0 & 1 & 0 & 0 \\ 0 & 0 & -\frac{gm_p}{m_v} & 0 \\ 0 & 0 & 0 & 1 \\ 0 & 1 & \frac{g(m_v + m_p)}{l_p m_v} & 0 \end{bmatrix} \begin{bmatrix} x_{1\delta} \\ x_{2\delta} \\ \theta_{1\delta} \\ \theta_{2\delta} \end{bmatrix} + \begin{bmatrix} 0 \\ -\frac{1}{m_v} \\ 0 \\ 1 \\ m_v + m_p \end{bmatrix} r_{2\delta}. \quad (27)$$

The subsystem (26) is the linear dynamical equation of the PVTOL's height with incremental control input $r_{1\delta}$. It is a fully actuated and controllable system; the control law will be proposed to accomplish a take-off and landing maneuver with an ADRC to compensate the nonlinearities neglected in the linearization process and external disturbances.

Similarly, the subsystem (27) is the PVTOL's horizontal position and the pendulum's angle linear dynamics with control input $r_{2\delta}$. It is an underactuated system. A control law by differential flatness approach will be developed for a rest-to-rest maneuver, and nonlinearities and external disturbances will be compensated by another ADRC. Both control proposals will be acting at same time to accomplish the control objectives.

3.2. Height Control

As mentioned earlier, system (26) is the linear dynamical equation of the PVTOL's height. The control objective is to achieve a take-off and landing maneuver. Consequently, we define the trajectory tracking error $e_y = y_d - y_{1\delta}$. Let us express the dynamical equation for trajectory tracking error in terms of state variables $e_{1y} = e_y$, and $e_{2y} = \dot{e}_y$, and the following dynamical equations are obtained:

$$\dot{e}_{1y} = e_{2y} \quad (28)$$

$$\dot{e}_{2y} = -\frac{r_{1\delta}}{m_v + m_p} - D_{y_d}. \quad (29)$$

By Assumption 1, \ddot{y}_d is not measurable, so it will be taken as disturbance. D_{y_d} represents the total disturbances by high-order terms neglected in linearization process, the possibly unmodeled dynamics and external disturbances by crosswind (23). D_{y_d} is considered uniformly absolutely bounded so $\|D_{y_d}\| < \delta_y$, with $\delta_y > 0$.

In order to reject the disturbance D_{y_d} , and to achieve Assumption 2, the following ESO is proposed for a simultaneous estimation of e_{2y} and disturbance signal D_{y_d} ,

$$\begin{aligned} \dot{\hat{e}}_{1y} &= \hat{e}_{2y} + \lambda_{1y}(e_{1y} - \hat{e}_{1y}) \\ \dot{\hat{e}}_{2y} &= u_2 + \lambda_{2y}(e_{1y} - \hat{e}_{1y}) + \hat{D}_{1y_d} \\ \dot{\hat{D}}_{1y_d} &= \hat{D}_{2y_d} + \lambda_{3y}(e_{1y} - \hat{e}_{1y}) \\ \dot{\hat{D}}_{2y_d} &= \lambda_{4y}(e_{1y} - \hat{e}_{1y}), \end{aligned} \quad (30)$$

where the state e_{1y} is measurable. The observation error of the state variable $O_y = e_{1y} - \hat{e}_{1y}$ generates the following linear reconstruction error dynamics:

$$O_y^4 + \lambda_{1y} O_y^3 + O_y^2 + O_y = \zeta_y.$$

The term ζ_y represents the total uniformly, absolutely bounded disturbance due to external and internal disturbances, i.e., $\|\zeta_y\| < \delta_2 \zeta$. To force the observation error O_y to be ultimately, uniformly, convergent toward a sufficiently small neighborhood of the

acceleration estimation error phase space, let us choose the observer control parameters, $\lambda_{jy} \ j = 1, 2, 3, 4$, such that the dominant linear injected error dynamics becomes stable (Hurwitz). The controller is thus given by

$$r_{1\delta} = (m_v + m_p)(-k_{y1}e_{1y} - k_{y2}\hat{e}_{2y} - \hat{D}_{1y_d}). \tag{31}$$

The trajectory tracking error dynamics of the closed loop is given by

$$\ddot{e}_y + k_{y2}\dot{e}_y + k_{y1}e_y = \eta_y.$$

where $\eta_y = \| D_{y_d} - \hat{D}_{y_d} \| < K_y$. The control parameters k_{y1} and k_{y2} are chosen such that a stable second-order dynamics with characteristic polynomial $s^2 + 2\omega_1\zeta_1s + \omega_1^2$, being $\omega_1, \zeta_1 \in \mathbb{R}^2$, is matched. In this case, the control parameters are chosen as $k_{y1} = \omega_1^2$ and $k_{y2} = 2\omega_1\zeta_1$. This means that the height y tends to be close to the desired trajectory y_d in a sufficiently small neighbourhood after a finite time t_y , so

$$\begin{aligned} \lim_{t \rightarrow \infty} |e_y| &< K_y \\ \lim_{t \rightarrow \infty} |r_{1\delta}| &< K_{r1}, \end{aligned}$$

where $K_{r1} > 0$.

3.3. Control for Horizontal Displacement and Pendulum's Angle

Considering the linear subsystem (x, θ) , described in equation (27), can be expressed in a compact form as

$$\dot{X}_{hp} = A_{hp}X_{hp} + B_{hp}r_{2\delta} \tag{32}$$

with

$$A_{hp} = \begin{bmatrix} 0 & 1 & 0 & 0 \\ 0 & 0 & -\frac{gm_p}{m_v} & 0 \\ 0 & 0 & 0 & 1 \\ 0 & 1 & \frac{g(m_v + m_p)}{l_p m_v} & 0 \end{bmatrix}; \quad B_{hp} = \begin{bmatrix} 0 \\ 1 \\ m_v \\ 1 \\ m_v + m_p \end{bmatrix}. \tag{33}$$

Moreover, $X_{hp} = (x_{1\delta}, x_{2\delta})^T$ and $r_{2\delta}$ as control input and according to [34,35], if the Kalman controllability matrix $C_k = [B_{hp} \ A_{hp}B_{hp} \ A_{hp}^2B_{hp} \ A_{hp}^3B_{hp}]$ is not singular, the pair (A_{hp}, B_{hp}) is controllable and hence the system is flat with flat output computed as

$$F = [0 \ 0 \ 0 \ 1]C_k^{-1}X_{hp}.$$

In order to simplify the calculation of the flat output time derivatives, flat output can be selected as

$$F = \Gamma[0 \ 0 \ 0 \ 1]C_k^{-1}X_{hp}$$

with $\Gamma = -\frac{g}{l_p^2 m}$ is a constant; defining the row vector

$$c_f = \Gamma[0 \ 0 \ 0 \ 1]C_k^{-1} \tag{34}$$

where flat output F and and a finite number of its time derivatives can be obtained with the following equation:

$$\begin{bmatrix} F \\ \dot{F} \\ \ddot{F} \\ F^{(3)} \end{bmatrix} = \begin{bmatrix} c_f \\ c_f A \\ c_f A^2 \\ c_f A^3 \end{bmatrix} X_{hp}. \quad (35)$$

Calculating (35), the flat output and its time derivative are completely parametrized in terms of the system variables and its time derivatives as

$$\begin{aligned} F &= \theta_{1\delta} - \frac{x_{1\delta}}{l_p} \\ \dot{F} &= \theta_{2\delta} - \frac{x_{2\delta}}{l_p} \\ \ddot{F} &= \frac{g\theta_{1\delta}}{l_p} \\ F^{(3)} &= \frac{g\theta_{2\delta}}{l_p}. \end{aligned} \quad (36)$$

The flat output fourth-order time derivative is obtained as follows:

$$F^{(4)} = \frac{g(-r_{2\delta} + g(m + m_p)\theta_{1\delta})}{l_p^2 m_v}.$$

Notice that the second and third time derivatives of flat outputs are computed by linear and angular velocities of θ_δ and x_δ and under Assumption 2, the velocities are not available. This restriction will be compensated in the control design procedure.

In the same way, all state variables can be parameterized by differential functions of the flat output F and can be computed by using Equation (36), as follows:

$$\begin{aligned} x_{1\delta} &= -l_p F + \frac{l_p^2 \ddot{F}}{g} \\ x_{2\delta} &= -l_p \dot{F} + \frac{l_p^2 F^{(3)}}{g} \\ \theta_{1\delta} &= \frac{l_p \ddot{F}}{g} \\ \theta_{2\delta} &= \frac{l_p F^{(3)}}{g} \\ r_{2\delta} &= \frac{-l_p^2 m_v F^{(4)} + g(m_v + m_p)l_p \ddot{F}}{g}. \end{aligned} \quad (37)$$

The linearized system is clearly equivalent to the following input–output model

$$F^{(4)} = \frac{gl_p \ddot{F}(m_v + m_p) - gr_{2\delta}}{l_p^2 m_v}. \quad (38)$$

From the differential parametrization (36), it is clear that the tangent system naturally decomposes into a cascade connection of two independent blocks. The first is controlled by the incremental input $r_{2\delta}$ with the output given by flat output \ddot{F} which coincides with a constant factor $\frac{g}{l_p}$, with incremental angular position of the pendulum $\theta_{1\delta}$, i.e., $\ddot{F} = \theta_{1\delta} \frac{g}{l_p}$. Then, the signal $\theta_{1\delta} \frac{g}{l_p}$ acts as an auxiliary control input to the second block, which consists of a chain of two integrators rendering the differential flat outputs \dot{F} and F . The last variable F is the output of the second block and the output to be controlled for the overall

system. This cascading property simplifies and decouples the observer design task in the flatness-based ADRC scheme.

Considering the system (38), we have the following simplified perturbed model for nonlinear subsystem (x, θ)

$$F^{(4)} = -\frac{g r_{2\delta}}{l_p^2 m_v} + \zeta_{x\theta}, \tag{39}$$

where $\zeta_{x\theta}$ represents state-dependent expressions, all the higher-order terms (h.o.t) neglected by the linearization, the possibly unmodeled dynamics, and external unknown disturbances affecting the system. All these uncertain terms are lumped into a single time-varying function represented by $\zeta_{x\theta}$ that is defined as

$$\zeta_{x\theta} = \frac{g l_p \ddot{F}(m_v + m_p)}{l_p^2 m_v} + h.o.t. \tag{40}$$

defining the auxiliary control input $r_{2\delta}$ as follows:

$$r_{2\delta} = -v_f \frac{l_p^2 m_v}{g}, \tag{41}$$

where v_f is a new control input. Let $F_i = F^{(i)}$, $i = 1, 2, 3, 4$, the flat perturbed state space model is given by

$$\begin{aligned} \dot{F}_1 &= F_2 \\ \dot{F}_2 &= F_3 \\ \dot{F}_3 &= F_4 \\ \dot{F}_4 &= v_f + \zeta_{x\theta}. \end{aligned} \tag{42}$$

At this point, the cascading property is used, which implies that we are to view the previous system as the connection of two subsystems (see Figure 3). Notice that F_3 corresponds to a measurable position, which can be measurable, and it is the known input to the second-order pure integration system

$$\begin{aligned} \dot{F}_1 &= F_2 \\ \dot{F}_2 &= F_3 \end{aligned}$$

and the remainder system is given by

$$\begin{aligned} \dot{F}_3 &= F_4 \\ \dot{F}_4 &= v_f + \zeta_{x\theta}. \end{aligned}$$

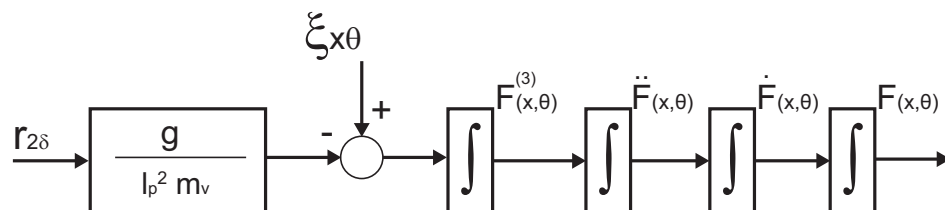


Figure 3. Cascade structure of (x, θ) sub-system.

The perturbation term $\zeta_{x\theta}$ can be expressed in terms of the input, the output, and their algebraic combination. Then it is algebraically observable [36]. Next, let us propose an instantaneous virtual evolution model of a time-polynomial nature for such a time-varying

function $\zeta_{x\theta}$, denoted by z , and adopt, say, the following third-order time polynomial model for $\zeta_{x\theta}$, i.e., $z^{(4)} = 0$. Then, with $z(t) = z_1$, the the flat perturbed state space model (42) can be rewritten as follows:

$$\begin{aligned}\dot{F}_i &= F_{i+1}, i = 1, 2, 3, \\ \dot{F}_4 &= v_f + z_1 \\ \dot{z}_j &= z_{j+1}, j = 1, 2, 3, \\ \dot{z}_4 &= 0.\end{aligned}\quad (43)$$

According to [33,37], a set of coupled, high-gain, extended linear Luenberger observers, for the simultaneous estimation of the phase variables associated with the flat output and the time-polynomial approximation variable, can be proposed as follows:

$$\begin{aligned}\dot{\hat{F}}_1 &= F_2 + k_1(F_1 - \hat{F}_1) \\ \dot{\hat{F}}_2 &= F_3 + k_2(F_1 - \hat{F}_1) \\ \dot{\hat{F}}_3 &= F_4 + \lambda_1(F_3 - \hat{F}_3) \\ \dot{\hat{F}}_4 &= v_f + \lambda_2(F_3 - \hat{F}_3) + \hat{z}_1 \\ \dot{\hat{z}}_1 &= \hat{z}_2 + \lambda_3(F_3 - \hat{F}_3) \\ \dot{\hat{z}}_2 &= \hat{z}_2 + \lambda_4(F_3 - \hat{F}_3) \\ \dot{\hat{z}}_3 &= \hat{z}_2 + \lambda_5(F_3 - \hat{F}_3) \\ \dot{\hat{z}}_4 &= \lambda_6(F_3 - \hat{F}_3).\end{aligned}\quad (44)$$

The observation error, $O_{F_1} = F_1 - \hat{F}_1$, of the incremental flat output, generates the following linear injected estimation error dynamics:

$$\ddot{O}_{F_1} + k_1\dot{O}_{F_1} + k_2O_{F_1} = 0.$$

An appropriate choice of observer parameters, k_1, k_2 such that the characteristic polynomial $s^2 + k_1s + k_2$ is Hurwitz renders an asymptotically, exponentially decreasing estimation error state. The tracking error velocity for the flat output \dot{O}_{F_1} is, thus, accurately estimated for feedback purposes.

In the same manner, considering the observation error $O_{F_3} = F_3 - \hat{F}_3$ of the flat output acceleration tracking error, it generates the following dominantly linear reconstruction error dynamics:

$$O_{F_3}^{(6)} + \lambda_1 O_{F_3}^{(5)} + \lambda_2 O_{F_3}^{(4)} + \lambda_3 O_{F_3}^{(3)} + \lambda_4 \ddot{O}_{F_3} + \lambda_5 \dot{O}_{F_3} + \lambda_6 O_{F_3} = \zeta_{x\theta}^{(4)}. \quad (45)$$

As stated in the previous ADRC designs, a necessary and sufficient condition for having the incremental flat output acceleration estimation error O_{F_3} and its time derivatives ultimately, uniformly, converge toward a small-as-desired neighborhood of the acceleration estimation error phase space is that $\zeta_{x\theta}^{(4)}$ be uniformly, absolutely bounded. An appropriate choice of observer gains coefficients: $\lambda_i, i = 1, 2, \dots, 6$, such that placing the poles of the associated linear homogeneous system sufficiently far into the left half of the complex plane, renders a uniformly, asymptotically convergent estimation error, O_{F_3} , toward an arbitrary small vicinity of the origin along with a finite number of its time derivatives.

The control input may then be readily synthesized with an active disturbance-cancelling strategy for the uncertain input $\zeta_{x\theta}$, in terms of the estimates value \hat{z}_1 and, for feedback purposes, of the estimated time derivatives associated with the incremental flat outputs F_1 and F_3 , both measurable. Then, the following control input v_f is proposed:

$$v_f = -K[F_1 \hat{F}_2 F_3 \hat{F}_4]^T - \hat{z}_1, \tag{46}$$

where F_1 and F_3 are used in a way that can be calculated through the variables x and θ , which are assumed to be measurable, \hat{F}_2 and \hat{F}_4 are estimates of F_2 and F_4 , and $K \in \mathbb{R}^{1 \times 4}$ is the gain matrix. Notice that the coefficients in K matrix must be chosen in accordance with the fact that, asymptotically, the flat output is being approximately governed by the differential equation

$$F_1^{(4)} + K_1 F_1^{(3)} + K_2 \ddot{F}_1 + K_3 \dot{F}_1 + K_4 F_1 = \zeta_{x\theta} - \hat{z}_1, \tag{47}$$

where the set of coefficients K_1, K_2, K_3, K_4 should render Hurwitz the following characteristic polynomial: $s^{(4)} + K_1 s^{(3)} + K_2 s^2 + K_3 s + K_4$. Finally, the diagram of the entire control scheme can be seen in Figure 4.

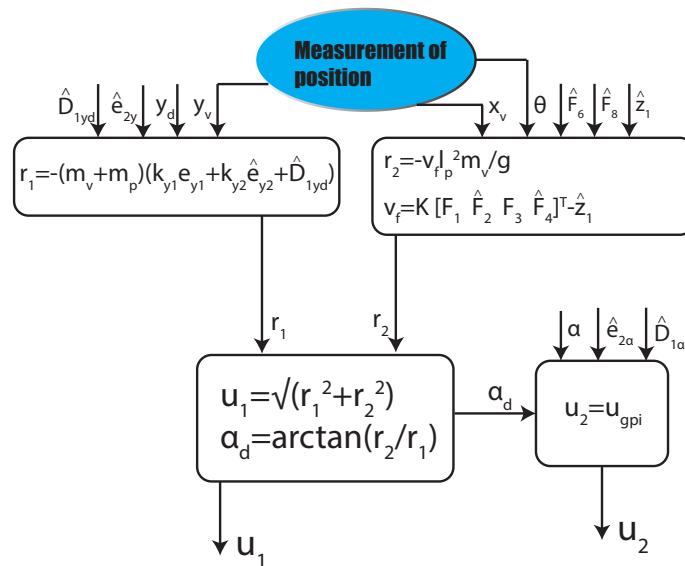


Figure 4. Diagram of the proposed control scheme.

4. Numerical Simulations

To test the controller’s performance, numerical simulations were carried out by using MATLAB–Simulink, and the results were obtained based on the numerical method of Runge–Kutta of the fourth order with a fixed step of 0.01 s. The physical parameters of the system are $m_v = 0.9$ kg, $m_p = 0.3$ kg, $l_p = 0.5$ m, $g = 9.81$ m/s². The desired trajectory in height position y_d was implemented by the use of *gauss2mf()* in Matlab software with the following parameters: $\sigma_1 = 1.5$, $\mu_1 = 10$, $\sigma_1 = 1.5$, and $\mu_1 = 20$.

The control parameters for u_2 (16) are proposed as $k_{\alpha 1} = 3.16$ and $k_{\alpha 2} = 2.7$, and the observers gain parameters (15) are calculated as follows:

$$\begin{aligned} \lambda_{1\alpha} &= 4\epsilon\omega_n \\ \lambda_{2\alpha} &= 2\omega_n^2 + 4\epsilon^2\omega_n^2 \\ \lambda_{3\alpha} &= 4\epsilon\omega_n^3 \\ \lambda_{4\alpha} &= \omega_n^4 \end{aligned} \tag{48}$$

with $\omega_n = 20$ and $\epsilon = 0.7$.

For the case of the controller $r_{1\delta}$ (31), the control parameters are set to be $k_{y1} = 3.16$ and $k_{y2} = 2.7$, and the observers gain parameters (30) are calculated according to the following expression:

$$\begin{aligned}
 \lambda_{1y} &= 4\epsilon\omega_n \\
 \lambda_{2y} &= 2\omega_n^2 + 4\epsilon^2\omega_n^2 \\
 \lambda_{3y} &= 4\epsilon\omega_n^3 \\
 \lambda_{4y} &= \omega_n^4
 \end{aligned} \tag{49}$$

with $\omega_n = 10$ and $\epsilon = 0.7$.

In the case of the controller v_f (46), the gain matrix K is proposed as

$$K = [1 \quad 3 \quad 4.2 \quad 3],$$

and the observers gain coefficients are calculated with the following equations:

$$\begin{aligned}
 k_1 &= 2\epsilon\omega_n \\
 k_2 &= \omega_n^2
 \end{aligned} \tag{50}$$

with $\omega_n = 10$ and $\epsilon = 0.7$

$$\begin{aligned}
 \lambda_1 &= 6\epsilon\omega_n \\
 \lambda_2 &= 3\omega_n^2 + 12\epsilon^2\omega_n^2 \\
 \lambda_3 &= 12\epsilon\omega_n^3 + 8\epsilon^3\omega_n^3 \\
 \lambda_4 &= 3\omega_n^4 + 12\epsilon^2\omega_n^4 \\
 \lambda_5 &= 6\epsilon\omega_n^5 \\
 \lambda_6 &= \omega_n^6
 \end{aligned} \tag{51}$$

with $\omega_n = 0.5$ and $\epsilon = 2$.

To show the effectiveness of the control scheme proposed in this work, a sliding mode control law was implemented to a comparison test against the robust differential flatness approach control scheme. The design of the sliding mode control is based on the linear approximation of the whole system that has the form (see Appendix A)

$$\dot{x}_L = A_L x_L + B_L u_L, \tag{52}$$

where A_L and B_L are the linear constant matrices of the tangent linearized system, $x_L = [x_v, \dot{x}_v, y_v, \dot{y}_v, \alpha, \dot{\alpha}, \theta, \dot{\theta}]^T$ are the state variables of the system, and $u_L = [u_1 \quad u_2]^T$ is the set of control inputs of the linearized system. The proposed sliding mode control is

$$u_1 = -5\text{sign}(K_{L1}x_L) \tag{53}$$

$$u_2 = -15\text{sign}(K_{L2}x_L), \tag{54}$$

where K_{L1} and K_{L2} are gain matrices designed by LQR technique based on the linearized system and $\text{sign}(x)$ is the sign function defined as follows:

$$\text{sign}(x) = \begin{cases} 1 & \text{if } x > 0 \\ -1 & \text{if } x < 0 \\ 0 & \text{if } x = 0 \end{cases} \tag{55}$$

and the matrices K_{L1} and K_{L2} are

$$K_{L1} = [0 \quad 0 \quad 1 \quad 1.8 \quad 0 \quad 0 \quad 0 \quad 0] \tag{56}$$

$$K_{L2} = [119 \quad 15.5 \quad 0 \quad 0 \quad 1 \quad 2.3 \quad -141 \quad -28]. \tag{57}$$

Both control laws were implemented in order to contrast the performance of the proposed control scheme with external disturbances caused by crosswind [30]. The crosswind dynamics are governed by the values of d_x , d_y and d_a . These values are proposed as random bounded numbers with a Gaussian distribution as follows:

$$\begin{aligned}d_x &= 0.5\text{rand}(t) \\d_y &= \text{rand}(t) \\d_a &= 0.5\text{rand}(t),\end{aligned}$$

where $\text{rand}()$ is a function that provides a random number in the interval $(-1, 1)$ with the Gaussian distribution.

Figure 5 shows the behavior of α with the proposed control scheme (—) and with sliding mode control (— · —). As can be seen, at the beginning of the simulation, the proposed control scheme shows a lesser overshooting effect than the sliding mode control response, and, in general, the error amplitude in the proposed control scheme is more reduced than the sliding mode case. This fact is shown in Figure 6 where an integral square error performance index of α is calculated for both cases.

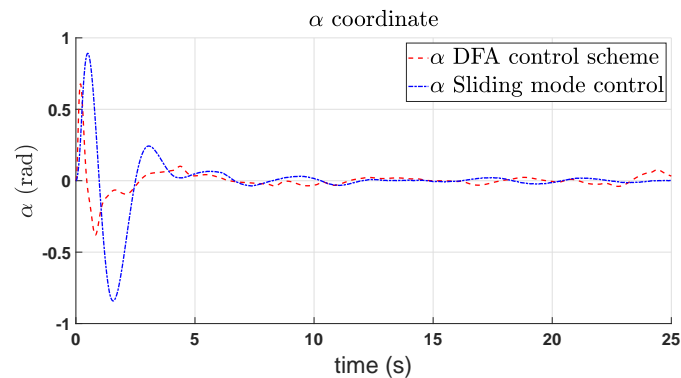


Figure 5. Behavior of α .

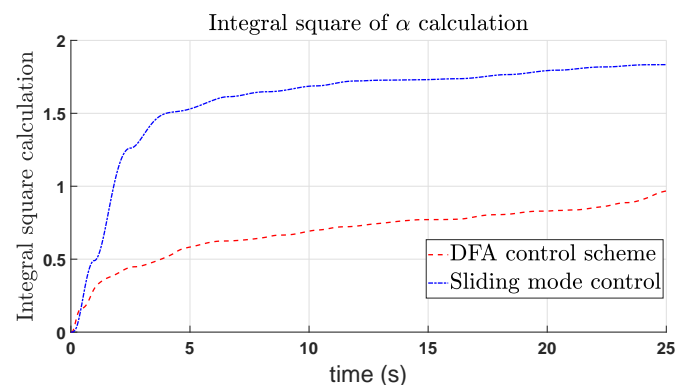


Figure 6. Integral square error index of α tracking.

Figure 7 shows the control input u_2 in both cases, for the proposed control scheme (—) and the sliding mode control (— · —). The chattering problem in sliding mode control does not appear, but a peaking phenomenon arises in the transient response of the sliding mode controller and a larger control amplitude of the proposal is noticed in the transient behavior due to the high gain nature of the controller. In Figure 7c, the energy consumption performance of u_2 , in both cases, is evaluated by calculating the integral square of u_2 . In this, it is evident that the behavior of the proposed controller u_2 demands less energy than the discontinuous proposal in steady state.

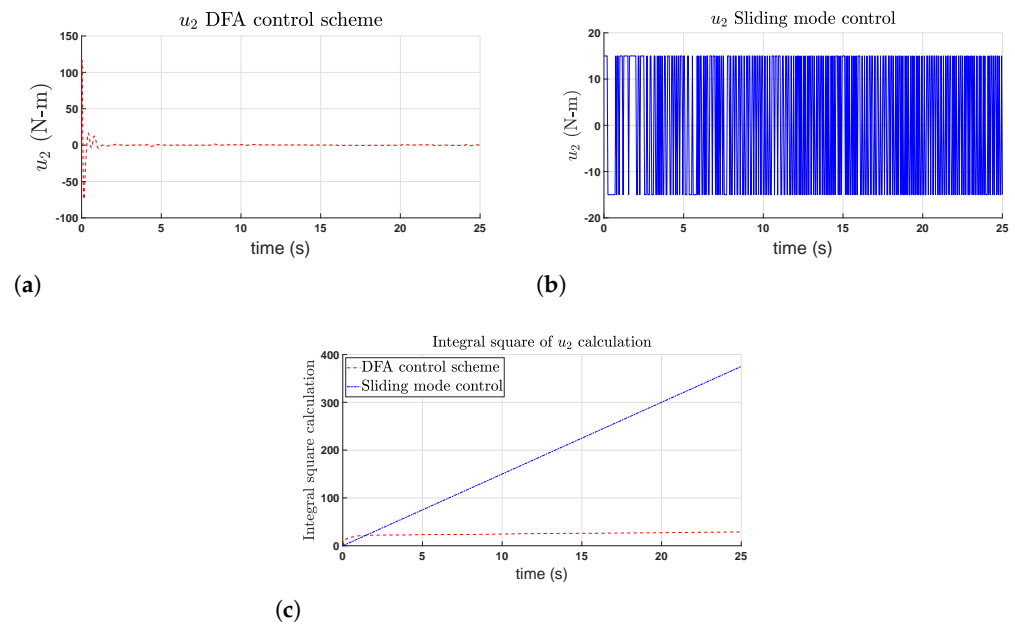


Figure 7. u_2 behavior results. (a) u_2 behavior (proposed control); (b) u_2 behavior (sliding mode control); (c) integral square of u_2 calculation.

Figure 8 shows the behavior of y_v with the proposed control scheme (—) and with sliding mode control (— · —), including the reference trajectory y_d (—). The proposal has a better transient behavior than the sliding mode, which can be seen in Figure 9. After a while, the tracking trajectory error in both cases are similar in amplitude, which shows that both controllers are suitable for the task. Controller u_1 's behavior with the proposed control scheme and with sliding mode are shown in Figure 10; in this case, the minimum and maximum amplitude of the proposed control is similar with respect to the sliding mode behavior. However, the discontinuous nature of the sliding mode control makes the integral square index of u_1 show less energy consumption of the proposal while ensuring competitive error results.

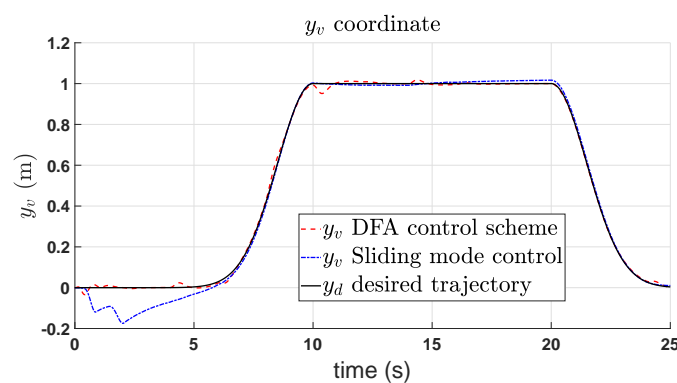


Figure 8. Behavior of y_v with the proposed control scheme and with the sliding mode control in trajectory tracking task.

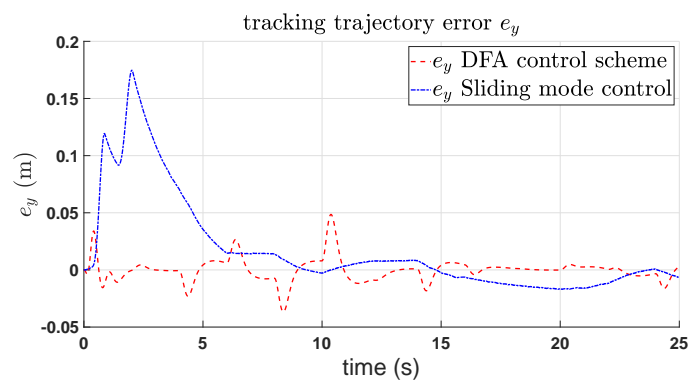


Figure 9. Tracking error behavior of e_y with the proposed controller and with the sliding mode control.

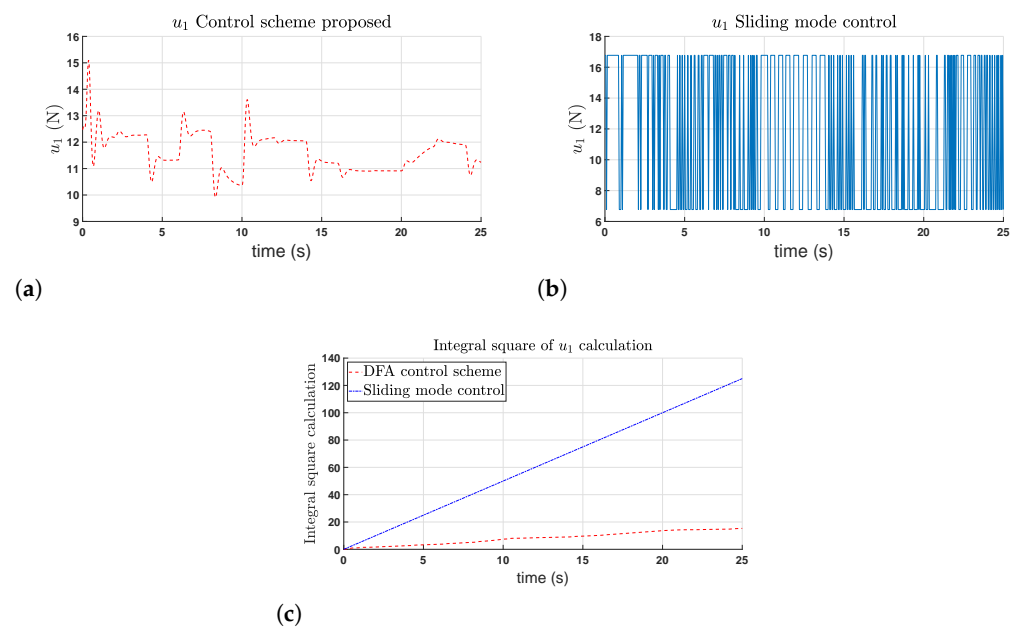


Figure 10. u_1 behavior for the implemented control schemes. (a) u_1 behavior (proposed control); (b) u_1 behavior (sliding mode control); (c) integral square index of u_1 .

The behavior of the coordinate x_v is shown in Figure 11 and the behavior of the pendulum's angle θ is shown in Figure 12. Physically, controller v_f moves the PVTOL system horizontally to keep the θ angle close to zero. The controller returns a horizontal displacement to zero at the same time to try to hold θ close to zero. In both coordinates, it is easy to see that the overshoot of the control proposal is less than the one exhibited by the sliding mode control but, after the overshoot phenomenon, the sliding mode control case has a lesser amplitude than the proposed control scheme.

The dynamics of the observation errors in the designed ESO (O_{α} , O_y , O_{F_3} and O_{F_5}), can be seen in Figures 13–16 respectively. In all cases, it is clear that the dynamics of observation errors converge to a close region of zero as expected.

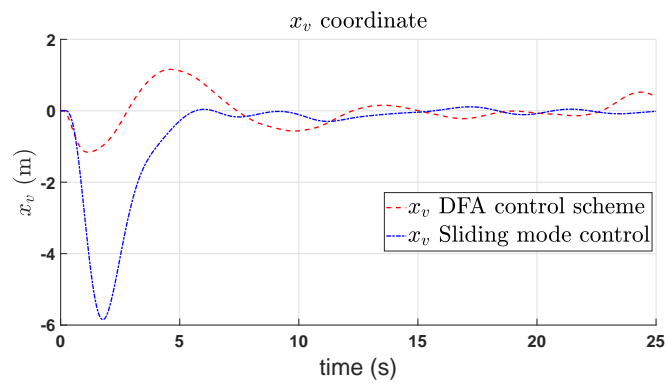


Figure 11. Behavior of x_v for the implemented control schemes.

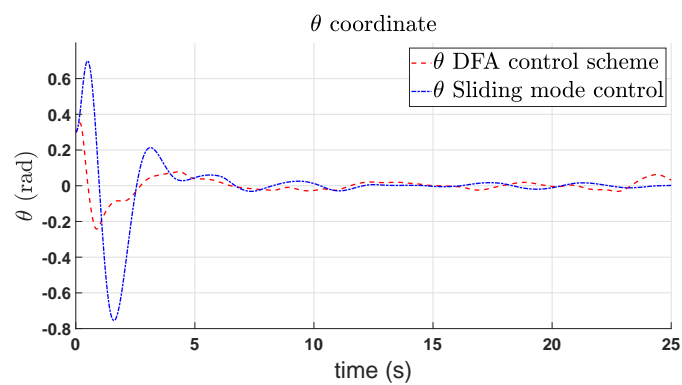


Figure 12. Behavior for θ for the implemented control schemes.

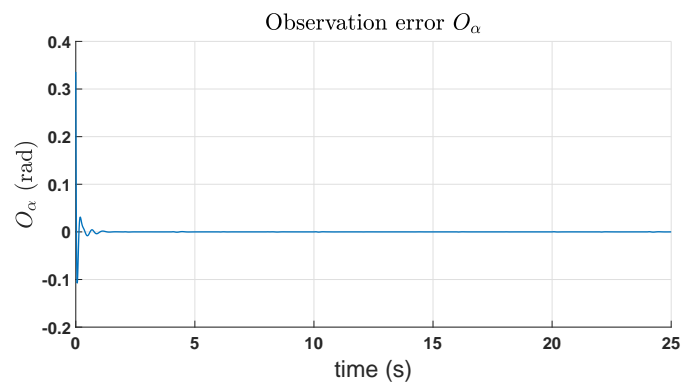


Figure 13. Observation error dynamics O_α .

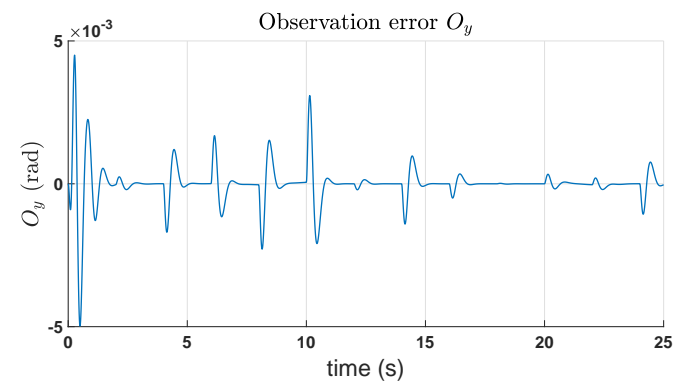


Figure 14. Observation error dynamics O_y .

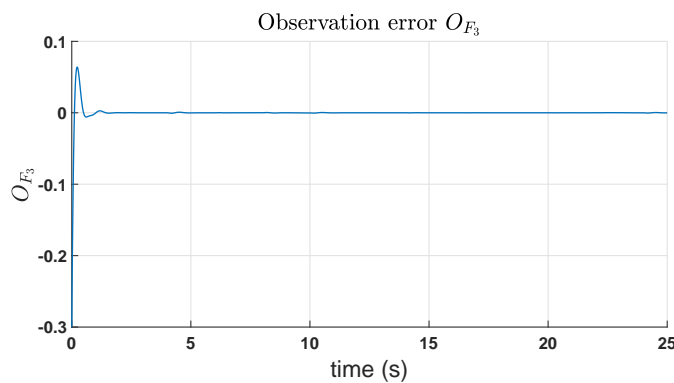


Figure 15. Observation error dynamics O_{F_3} .

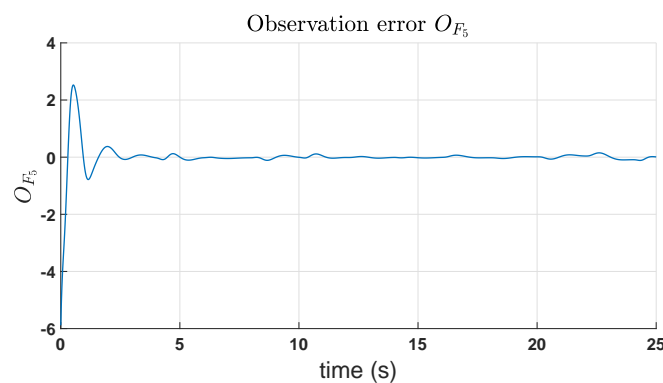


Figure 16. Observation error dynamics O_{F_5} .

5. Conclusions

This work presents a control scheme for a PVTOL aircraft system with an inverted pendular load. This control scheme is divided into three control loops. The first closed-loop control is focused on a trajectory tracking for α angle in order to use the desired trajectory α_d as an artificial control. An ADRC controller is proposed in order to reject internal and external disturbances and unknown derivatives as well. After defining auxiliary control inputs, the PVTOL aircraft system with an inverted pendular load is tangentially linearized around the unstable equilibrium point. The linearized PVTOL aircraft system with an inverted pendular load is divided into two subsystems: the height system and the horizontal pendulum system.

In the height system, an ADRC controller is proposed in terms of the trajectory tracking error to achieve take-off and landing maneuvers in the presence of external disturbances. The third closed-loop control is designed by means of exploiting the flatness associated with the linearized model and via an extended state observer-based linear ADRC.

This control scheme achieves a competitive robustness in the presence of external disturbances, due to crosswind, and to reject the nonlinearities of the PVTOL aircraft system with an inverted pendular load model, neglected in the linearization process, which means that the proposed controller behaves well even in this undesirable realistic scenario. It is important to note that the scheme achieves greatly competitive numerical simulation results when compared with another effective robust controller, the sliding mode control. Note that the performance index of both controllers was computed to compare them, and the outcome revealed that our strategy has a better performance than the sliding mode controller.

Author Contributions: Conceptualization, C.A.V.R., A.L.-J., N.B.L.-C., B.E.C.-G., D.M.-V., and O.G.-F.; methodology, C.A.V.R., A.L.-J., N.B.L.-C., B.E.C.-G., D.M.-V., and O.G.-F.; software, C.A.V.R., A.L.-J., N.B.L.-C., B.E.C.-G., D.M.-V., and O.G.-F.; validation, C.A.V.R., A.L.-J., N.B.L.-C., B.E.C.-G., D.M.-V., and O.G.-F.; writing—original draft preparation, C.A.V.R., A.L.-J., and O.G.-F.; writing—review and editing, C.A.V.R., A.L.-J., N.B.L.-C., B.E.C.-G., D.M.-V., and O.G.-F.; visualization, A.L.-J.

and N.B.L.-C.; funding acquisition, A.L.-J., N.B.L.-C., B.E.C.-G., and O.G.-F. All authors have read and agreed to the published version of the manuscript.

Funding: This research was funded by Secretaría de Investigación y Posgrado del Instituto Politécnico Nacional (SIP-IPN) under grant numbers 20220542, 20220632, 20220623 and 20220633.

Institutional Review Board Statement: Not applicable.

Informed Consent Statement: Not applicable.

Data Availability Statement: Not applicable.

Acknowledgments: C. Alejandro Villaseñor Rios thanks the support from the CONACYT.

Conflicts of Interest: The authors declare no conflict of interest.

Appendix A. Design of the Sliding Mode Control

The design of sliding mode control is based on linear approximation of the whole system that has the form

$$\dot{x}_L = A_L x_L + B_L u_L \tag{A1}$$

where A_L and B_L are the linear constant matrices of the linearized system by Taylor series, $x_L = (y_\delta, \dot{y}_\delta, \alpha_\delta, \dot{\alpha}_\delta, x_\delta, \dot{x}_\delta, \theta_\delta, \dot{\theta}_\delta)^\top$ are the incremental variables states of the linearized system and $u_L = (u_1, u_2)$ is the set of control inputs of the linearized system, and the matrices of the tangent linearized system (A1) are:

$$A_L = \begin{bmatrix} 0 & 1 & 0 & 0 & 0 & 0 & 0 & 0 \\ 0 & 0 & 0 & 0 & 0 & 0 & 0 & 0 \\ 0 & 0 & 0 & 1 & 0 & 0 & 0 & 0 \\ 0 & 0 & 0 & 0 & 0 & 0 & 0 & 0 \\ 0 & 0 & 0 & 0 & 0 & 1 & 0 & 0 \\ 0 & 0 & -\frac{g(m_v+mp)}{m} & 0 & 0 & 0 & \frac{g(m_v+mp)}{m_v} & 0 \\ 0 & 0 & 0 & 0 & 0 & 0 & 0 & 1 \\ 0 & 0 & -\frac{g(m_v+mp)}{lpm} & 0 & 0 & 0 & \frac{g(m_v+mp)}{lpm_v} & 0 \end{bmatrix} \quad B_L = \begin{bmatrix} 0 & 0 \\ \frac{1}{m_v+mp} & 0 \\ 0 & 0 \\ 0 & 1 \\ 0 & 0 \\ 0 & 0 \\ 0 & 0 \\ 0 & 0 \end{bmatrix}$$

The height dynamics is decoupled of the rest of the system with u_1 as control input, so; for which it is possible to separate the dynamics in the linear system in the following way.

$$\dot{x}_{Lh} = A_{Lh} x_{Lh} + B_{Lh} u_1 \tag{A2}$$

$$A_{Lh} = \begin{bmatrix} 0 & 1 \\ 0 & 0 \end{bmatrix} \quad B_{Lh} = \begin{bmatrix} 0 \\ \frac{1}{m_v+mp} \end{bmatrix}$$

$$\dot{x}_{L\theta} = A_{L\theta} x_{L\theta} + B_{L\theta} u_2 \tag{A3}$$

$$A_{L\theta} = \begin{bmatrix} 0 & 1 & 0 & 0 & 0 & 0 \\ 0 & 0 & 0 & 0 & 0 & 0 \\ 0 & 0 & 0 & 1 & 0 & 0 \\ -\frac{g(m_v+mp)}{m} & 0 & 0 & 0 & \frac{g(m_v+mp)}{m} & 0 \\ 0 & 0 & 0 & 0 & 0 & 1 \\ -\frac{g(m_v+mp)}{lpm} & 0 & 0 & 0 & \frac{g(m_v+mp)}{lpm} & 0 \end{bmatrix} \quad B_{L\theta} = \begin{bmatrix} 0 \\ 1 \\ 0 \\ 0 \\ 0 \\ 0 \end{bmatrix}$$

where $x_{Lh} = (y_\delta, \dot{y}_\delta) = (y_1, y_2)$ is the state variable for height dynamics with A_{Lh} and B_{Lh} linear matrices of the system and u_1 as control input; $x_{L\theta} = (\alpha_\delta, \dot{\alpha}_\delta, x_\delta, \dot{x}_\delta, \theta_\delta, \dot{\theta}_\delta) =$

$(\alpha_1, \alpha_2, x_1, x_2, \theta_1, \theta_2)$ is the state variable for $(\alpha_\delta, x_\delta, \theta_\delta)$ dynamics with $A_{L\theta}$ and $B_{L\theta}$ linear matrices and u_2 as control input. The sliding mode control proposed is

$$u_1 = -v_1 \text{sign}(K_{L1}x_{Lh}) + g(m_v + m_p) \quad (\text{A4})$$

$$u_2 = -v_2 \text{sign}(K_{L2}x_{l\theta}) \quad (\text{A5})$$

where v_1 and v_2 are control gains and K_{L1} and K_{L2} are gain matrices designed by the LQR technique based on the linearized system with $\text{lqr}()$ MATLAB function as follows

$$K_{L1} = \text{lqr}(A_{Lh}, B_{Lh}, \text{eye}(2), 1)$$

$$K_{L2} = \text{lqr}(A_{L\theta}, B_{L\theta}, \text{eye}(6), 1)$$

$\text{sign}(x)$ is the sign function defined as follows

$$\text{sign}(x) = \begin{cases} 1 & \text{if } x > 0 \\ -1 & \text{if } x < 0 \\ 0 & \text{if } x = 0 \end{cases} \quad (\text{A6})$$

The stability proof for whole system is divided in two steps: stability proof for (A2) system and stability proof for (A3) system.

Appendix A.1. Stability Proof for Height Dynamics

To proof the height dynamics (A2) stability in closed loop with the control u_2 (A5), let us take the following sliding mode surface

$$\sigma_y = K_{L1}x_{Lh} = K_{L11}y_1 + K_{L12}y_2$$

Defining the following Lyapunov function

$$V_y = \frac{1}{2}\sigma_y^2$$

taking the time derivative of V_y yields

$$\dot{V}_y = \sigma_y \dot{\sigma}_y = \sigma_y(K_{L11}\dot{y}_1 + K_{L12}\dot{y}_2)$$

$$\dot{V}_y = \sigma_y(K_{L11}y_2 + K_{L12}\left(\frac{u_{1\delta}}{m_v + m_p} + \epsilon_y\right))$$

$$\dot{V}_y = \sigma_y(K_{L11}y_2 + K_{L12}\left(\frac{-v_1 \text{sign}(\sigma_y) + g(m_v + m_p)}{m_v + m_p} + \epsilon_y\right))$$

$$\dot{V}_y = \sigma_y(K_{L11}y_2 + K_{L12}(-C_1 \text{sign}(\sigma_y) + g + \epsilon_y))$$

$$\dot{V}_y = \sigma_y(-P_y \text{sign}(\sigma_y) + \zeta_y)$$

where ζ_y represents the total disturbance in y_v dynamics with other terms that may affect in stability, and must be bounded so $\zeta_y \leq L_y$; P_y is a new control parameter.

$$\dot{V}_y \leq \sigma_y(-P_y \text{sign}(\sigma_y) + L_y)$$

$$\dot{V}_y \leq -P_y |\sigma_y| + \sigma_y L_y \leq -P_y |\sigma_y| + |\sigma_y| L_y$$

if $P_y > L_y$ then $\dot{V}_y < 0$; so, the system is asymptotically stable at origin.

Appendix A.2. Stability Proof for (α, x_v, θ) Dynamics

To proof the (α, x_v, θ) dynamics (A3) stability in closed-loop with control u_1 (A4), let us take the following sliding surface

$$\sigma = K_{L2}x_{L2} = K_{L2_1}\alpha_1 + K_{L2_2}\alpha_2 + K_{L2_3}x_1 + K_{L2_4}x_2 + K_{L2_5}\theta_1 + K_{L2_6}\theta_2$$

Defining the following Lyapunov function

$$V = \frac{1}{2}\sigma^2$$

taking the time derivative of V yields

$$\dot{V} = \sigma\dot{\sigma} = \sigma(K_{L2_1}\dot{\alpha}_2 + K_{L2_2}\dot{\alpha}_2 + K_{L2_3}\dot{x}_2 + K_{L2_4}\dot{x}_2 + K_{L2_5}\dot{\theta}_2 + K_{L2_6}\dot{\theta}_2)$$

$$\dot{V} = \sigma(K_{L2_1}\alpha_2 + K_{L2_2}(-v_2\text{sign}(\sigma)) + K_{L2_3}x_2 + K_{L2_4}\dot{x}_2 + K_{L2_5}\theta_2 + K_{L2_6}\dot{\theta}_2)$$

$$\dot{V} = \sigma(-P_\theta\text{sign}(\sigma) + \xi_\theta)$$

where ξ_θ denotes the total disturbances in y_v dynamics with other terms that may affect in stability; and must be bounded, $\xi_y \leq L_\theta$; P_y is a new control parameter.

$$\dot{V} \leq \sigma(-P_\theta\text{sign}(\sigma) + L_\theta)$$

$$\dot{V} \leq -P_\theta |\sigma| + \sigma L_\theta \leq -P_\theta |\sigma| + |\sigma| L_\theta$$

if $P_\theta > L_\theta$ then $\dot{V} < 0$; so, the equilibrium given by the surface is asymptotically stable at the origin.

References

- Boubaker, O. The inverted pendulum: A fundamental benchmark in control theory and robotics. In Proceedings of the International Conference on Education and e-Learning Innovations, Sousse, Tunisia, 1–3 July 2012; pp. 1–6.
- Shkolnik, A.; Tedrake, R. High-dimensional underactuated motion planning via task space control. In Proceedings of the 2008 IEEE/RSJ International Conference on Intelligent Robots and Systems, Nice, France, 22–26 September 2008; pp. 3762–3768.
- Ramírez-Neria, M.; Sira-Ramírez, H.; Garrido-Moctezuma, R.; Luviano-Juarez, A. Linear active disturbance rejection control of underactuated systems: The case of the Furuta pendulum. *ISA Trans.* **2014**, *53*, 920–928. [[CrossRef](#)] [[PubMed](#)]
- Gómez-Estern, F.; Van der Schaft, A.J. Physical damping in IDA-PBC controlled underactuated mechanical systems. *Eur. J. Control.* **2004**, *10*, 451–468. [[CrossRef](#)]
- Jabbari Asl, H.; Oriolo, G.; Bolandi, H. Output feedback image-based visual servoing control of an underactuated unmanned aerial vehicle. *Proc. Inst. Mech. Eng. Part I J. Syst. Control. Eng.* **2014**, *228*, 435–448. [[CrossRef](#)]
- Rodríguez-Seda, E.J.; Tang, C.; Spong, M.W.; Stipanović, D.M. Trajectory tracking with collision avoidance for nonholonomic vehicles with acceleration constraints and limited sensing. *Int. J. Robot. Res.* **2014**, *33*, 1569–1592. [[CrossRef](#)]
- Ramírez-Neria, M.; Ochoa-Ortega, G.; Lozada-Castillo, N.; Trujano-Cabrera, M.A.; Campos-Lopez, J.P.; Luviano-Juárez, A. On the robust trajectory tracking task for flexible-joint robotic arm with unmodeled dynamics. *IEEE Access* **2016**, *4*, 7816–7827. [[CrossRef](#)]
- Furut, K.; Ochiai, T.; Ono, N. Attitude control of a triple inverted pendulum. *Int. J. Control* **1984**, *39*, 1351–1365. [[CrossRef](#)]
- Haddad, N.K.; Chemori, A.; Belghith, S. Robustness enhancement of IDA-PBC controller in stabilising the inertia wheel inverted pendulum: theory and real-time experiments. *Int. J. Control* **2018**, *91*, 2657–2672. [[CrossRef](#)]
- Fantoni, I.; Lozano, R. Global stabilization of the cart-pendulum system using saturation functions. In Proceedings of the 42nd IEEE International Conference on Decision and Control (IEEE Cat. No. 03CH37475), Maui, HI, USA, 9–12 December 2003; Volume 5, pp. 4393–4398.
- Aguilar-Ibañez, C.; Suárez-Castañón, M.S.; Gutiérrez-Frias, O.O. The direct Lyapunov method for the stabilisation of the Furuta pendulum. *Int. J. Control* **2010**, *83*, 2285–2293. [[CrossRef](#)]
- Moeini, A.; Lynch, A.F.; Zhao, Q. A backstepping disturbance observer control for multirotor UAVs: theory and experiment. *Int. J. Control* **2021**. [[CrossRef](#)]
- Hua, M.D.; Hamel, T.; Morin, P.; Samson, C. Introduction to feedback control of underactuated VTOL vehicles: A review of basic control design ideas and principles. *IEEE Control. Syst. Mag.* **2013**, *33*, 61–75.
- Liu, C.; Pan, J.; Chang, Y. PID and LQR trajectory tracking control for an unmanned quadrotor helicopter: Experimental studies. In Proceedings of the 2016 35th Chinese Control Conference (CCC), Chengdu, China, 27–29 July 2016; pp. 10845–10850.

15. Xiong, L.; Yu, Z.; Wang, Y.; Yang, C.; Meng, Y. Vehicle dynamics control of four in-wheel motor drive electric vehicle using gain scheduling based on tyre cornering stiffness estimation. *Veh. Syst. Dyn.* **2012**, *50*, 831–846. [[CrossRef](#)]
16. Lozano Hernández, Y.; Gutiérrez Frías, O.; Lozada-Castillo, N.; Luviano Juárez, A. Control algorithm for taking off and landing manoeuvres of quadrotors in open navigation environments. *Int. J. Control. Autom. Syst.* **2019**, *17*, 2331–2342. [[CrossRef](#)]
17. Azinheira, J.R.; Moutinho, A. Hover control of an UAV with backstepping design including input saturations. *IEEE Trans. Control. Syst. Technol.* **2008**, *16*, 517–526. [[CrossRef](#)]
18. Das, A.; Lewis, F.; Subbarao, K. Backstepping approach for controlling a quadrotor using lagrange form dynamics. *J. Intell. Robot. Syst.* **2009**, *56*, 127–151. [[CrossRef](#)]
19. Zheng, E.H.; Xiong, J.J.; Luo, J.L. Second order sliding mode control for a quadrotor UAV. *ISA Trans.* **2014**, *53*, 1350–1356. [[CrossRef](#)] [[PubMed](#)]
20. Hauser, J.; Sastry, S.; Meyer, G. Nonlinear control design for slightly non-minimum phase systems: Application to V/STOL aircraft. *Automatica* **1992**, *28*, 665–679. [[CrossRef](#)]
21. Escobar, J.C.; Lozano, R.; Bonilla Estrada, M. PVTOL control using feedback linearisation with dynamic extension. *Int. J. Control* **2021**, *94*, 1794–1803. [[CrossRef](#)]
22. Zavala-Río, A.; Fantoni, I.; Lozano, R. Global stabilization of a PVTOL aircraft model with bounded inputs. *Int. J. Control* **2003**, *76*, 1833–1844. [[CrossRef](#)]
23. López-Araujo, D.J.; Zavala-Río, A.; Fantoni, I.; Salazar, S.; Lozano, R. Global stabilisation of the PVTOL aircraft with lateral force coupling and bounded inputs. *Int. J. Control* **2010**, *83*, 1427–1441. [[CrossRef](#)]
24. Aguilar-Ibanez, C.; Suarez-Castanon, M.S.; Meda-Campaña, J.; Gutierrez-Frias, O.; Merlo-Zapata, C.; Martinez-Castro, J.A. A simple approach to regulate a pvtol system using matching conditions. *J. Intell. Robot. Syst.* **2020**, *98*, 511–524. [[CrossRef](#)]
25. Munoz, L.E.; Santos, O.; Castillo, P. Robust nonlinear real-time control strategy to stabilize a PVTOL aircraft in crosswind. In Proceedings of the 2010 IEEE/RSJ International Conference on Intelligent Robots and Systems, Taipei, Taiwan, 18–22 October 2010; pp. 1606–1611.
26. Hehn, M.; D’Andrea, R. A flying inverted pendulum. In Proceedings of the 2011 IEEE International Conference on Robotics and Automation, Shanghai, China, 9–13 May 2011; pp. 763–770.
27. Krafes, S.; Chalh, Z.; Saka, A. Vision-based control of a flying spherical inverted pendulum. In Proceedings of the 2018 4th International Conference on Optimization and Applications (ICOA), Mohammedia, Morocco, 26–27 April 2018; pp. 1–6.
28. Chen, H.; Yang, Y.; Sun, J. Improved Genetic Algorithm Based Optimal Control for A Flying Inverted Pendulum. In Proceedings of the 2019 3rd International Conference on Electronic Information Technology and Computer Engineering (EITCE), Xiamen, China, 18–20 October 2019; pp. 1428–1432.
29. Nayak, A.; Banavar, R.N.; Maithripala, D. Stabilizing a spherical pendulum on a quadrotor. *Asian J. Control* **2020**, *24*, 1112–1121. [[CrossRef](#)]
30. Aguilar-Ibanez, C.; Sira-Ramirez, H.; Suarez-Castanon, M.S.; Garrido, R. Robust trajectory-tracking control of a PVTOL under crosswind. *Asian J. Control* **2019**, *21*, 1293–1306. [[CrossRef](#)]
31. Zhang, C.; Hu, H.; Gu, D.; Wang, J. Cascaded control for balancing an inverted pendulum on a flying quadrotor. *Robotica* **2017**, *35*, 1263–1279. [[CrossRef](#)]
32. Ramírez-Neria, M.; Sira-Ramírez, H.; Garrido-Moctezuma, R.; Luviano-Juárez, A. Active disturbance rejection control of the inertia wheel pendulum through a tangent linearization approach. *Int. J. Control. Autom. Syst.* **2019**, *17*, 18–28. [[CrossRef](#)]
33. Ramírez-Neria, M.; Sira-Ramírez, H.; Garrido-Moctezuma, R.; Luviano-Juárez, A. On the linear control of underactuated nonlinear systems via tangent flatness and active disturbance rejection control: The case of the ball and beam system. *J. Dyn. Syst. Meas. Control* **2016**, *138*, 104501. [[CrossRef](#)]
34. Sira-Ramirez, H.; Agrawal, S.K. *Differentially Flat systems*; Crc Press: Boca Raton, FL, USA, 2018.
35. Sira-Ramírez, H.; Luviano-Juárez, A.; Ramírez-Neria, M.; Zurita-Bustamante, E.W. *Active Disturbance Rejection Control of Dynamic Systems: A Flatness Based Approach*; Butterworth-Heinemann: Oxford, UK, 2018.
36. Diop, S.; Fliess, M. Nonlinear observability, identifiability, and persistent trajectories. In Proceedings of the 30th IEEE Conference on Decision and Control, Brighton, UK, 11–13 December 1991; pp. 714–719.
37. Ramírez-Neria, M.; Sira-Ramírez, H.; Garrido-Moctezuma, R.; Luviano-Juárez, A.; Gao, Z. Active Disturbance Rejection Control for Reference Trajectory Tracking Tasks in the Pendubot System. *IEEE Access* **2021**, *9*, 102663–102670. [[CrossRef](#)]